Seasonal variation of thermospheric density and composition

Liying Qian,[1] Stanley C. Solomon,[1] and Timothy J. Kane[2]

[1] Thermospheric neutral density and composition exhibit a strong seasonal variation, with maxima near the equinoxes, a primary minimum during northern hemisphere summer, and a secondary minimum during southern hemisphere summer. This pattern of variation is described by thermospheric empirical models. However, the mechanisms are not well understood. The annual insolation variation due to the Sun-Earth distance can cause an annual variation, large-scale interhemispheric circulation can cause a global semiannual variation, and geomagnetic activity can also have a small contribution to the semiannual amplitude. However, simulations by the National Center for Atmospheric Research (NCAR) Thermosphere-Ionosphere-Electrodynamics General Circulation Model (TIE-GCM) indicates that these seasonal effects do not fully account for the observed annual/semiannual amplitude, primarily because of the lack of a minimum during northern hemisphere summer. A candidate for causing this variation is a change in composition, driven by eddy mixing in the mesopause region. Other observations and model studies suggest that eddy diffusion in the mesopause region has a strong seasonal variation, with eddy diffusion larger during solstices than equinoxes, and stronger turbulence in summer than in winter. A seasonal variation of eddy diffusion compatible with this description is obtained. Simulations show that when this function is imposed at the lower boundary of the TIE-GCM, neutral density variation consistent with satellite drag data and O/N_2 consistent with measurements by TIMED/GUVI, are obtained. These model-data comparisons and analyses indicate that turbulent mixing originated from the lower atmosphere may contribute to seasonal variation in the thermosphere, particularly the asymmetry between solstices that cannot be explained by other mechanisms.

Citation: Qian, L., S. C. Solomon, and T. J. Kane (2009), Seasonal variation of thermospheric density and composition, *J. Geophys. Res.*, *114*, A01312, doi:10.1029/2008JA013643.

1. Introduction

[2] An important goal for numerical and empirical modeling of the thermosphere-ionosphere system is to obtain accurate descriptions of thermospheric density in response to solar irradiance variation and magnetospheric activity, because of the changes in satellite orbits induced by atmospheric drag. Between the timescales of the 11-year solar cycle and episodic solar and geomagnetic events, it is important to fully characterize the seasonal behavior of the thermosphere, both in regard to its spatial distribution of density and composition, and its global mean behavior. Although these seasonal changes have been observed for decades using a variety of measurements, there is surprisingly little convergence on a full theoretical understanding of the causes.

[3] The annual thermospheric density variation was first observed by *Paetzold and Zschörner* [1961] through analysis of satellite drag data. They found that neutral density has a minimum from May to August and a broad maximum during the rest of the year with a secondary minimum near January. The magnitude of the annual minimum to maximum variation is more than 100%. Using harmonic analysis, they further found that the annual variation is a semiannual variation superimposed on an annual variation, and the ratio of the amplitude of the annual to semiannual variation is 3:2. Since this amplitude is too large to be explained by the annual insolation variation due to the Sun-Earth distance, they suggested that the annual and semiannual variation could be caused by interaction of the terrestrial upper atmosphere with interplanetary matter. This pattern of neutral density is often referred to as semiannual density variation, despite the dominance of the annual term. In this work, we refer to this pattern of density variation as ''annual/semiannual'' or ''seasonal'' and use the term ''semiannual'' to refer specifically to the semiannual component.

[4] *Jacchia* [1965] represented annual/semiannual density variation with temperature functions in his 1965 thermospheric empirical density model (J65). However, difficulty arose when the J65 annual/semiannual density variation showed a large discrepancy with drag data from satellites having altitudes beyond the range of 250 km to 600 km [*Cook*, 1967, 1969], the altitude range of data upon which

[1]High Altitude Observatory, National Center for Atmospheric Research, Boulder, Colorado, USA.
[2]Department of Electrical Engineering, Pennsylvania State University, University Park, Pennsylvania, USA.

J65 was based. *Jacchia* [1971] then reappraised the J65 model's approach to annual/semiannual density variation and suggested that it can be represented as a pure density variation with amplitude as a function of height. The annual/semiannual density variation employed in the Jacchia model shows maxima in April and October, a primary minimum in July, and a secondary minimum in January.

[5] The MSIS series of models [*Hedin et al.*, 1977a, 1977b; *Hedin*, 1983, 1987, 1991; *Picone et al.*, 2002] represent annual/semiannual density variation with a combined contribution from temperature and composition variation. The composition function is imposed at 120 km and propagates to the upper thermosphere through molecular diffusion. Composition has a strong effect on density in the upper thermosphere because of the difference in atomic/molecular weight between the two principal thermospheric constituents, atomic oxygen and molecular nitrogen. Reduction in their ratio (O/N_2) has the effect of increasing mean molecular mass, and therefore, reduces density scale height, which in turn decreases mass density at a given altitude in the upper thermosphere.

[6] *Bowman* [2004] analyzed drag data from 13 satellites with perigee heights between 200 km and 1100 km to characterize the annual/semiannual density variation from 1970–2002. The satellites have either moderate eccentric orbits or nearly circular orbits, and have a variety of inclinations. He found that both the phase and amplitude of the annual/semiannual density variation change from year to year, with more complicated phase variation under high solar activity conditions. The amplitude increases with altitude from 200 km to ~800 km and then declines at higher altitudes. The amplitude variability with solar activity is small for low-earth orbit satellites, i.e., near 400 km, but the amplitude increases with solar activity at greater altitudes, and the amplitude can range between ~30% to as much as ~250%, depending on altitude and solar activity.

[7] Empirical models can reproduce the annual/semiannual density variation, but mechanisms for the variation are not addressed. The annual 7% variation of insolation due to variation of the Sun-Earth distance can result in an annual asymmetry, with terrestrial perihelion and hence maximum irradiance during January. However, *Paetzold and Zschörner* [1961] found that the resulting amplitude is too small compared to what was observed by satellite drag data. *Walterscheid* [1982] suggested that there is a globally averaged temperature variation between solstice and equinox because of stronger geomagnetic activity at equinoxes than solstices. However, the semiannual variation in geomagnetic activity is too small [*Detman*, 1996] to account for the large semiannual amplitude in density variation. The detection of composition anomalies, such as winter bulges of light species in the thermosphere [*Hedin and Alcaydé*, 1974; *Jacchia*, 1974; *Potter et al.*, 1977] and the depletion of O and He at high latitude during magnetic storms [*Taeusch et al.*, 1971; *Jacchia et al.*, 1976; *Jacchia*, 1977; *Prölss and von Zahn*, 1977], prompted attribution of latitudinal and seasonal variations in composition to large-scale interhemispheric circulation induced by the latitudinal gradient of heating by solar irradiance and geomagnetic storms [*Johnson and Gottlieb*, 1970; *Mayr and Volland*, 1971, 1972; *Mayr et al.*, 1978]. *Fuller-Rowell* [1998] further proposed that large-scale interhemispheric circulation is a mechanism for global semiannual density variation. Model simulations show that the large-scale interhemispheric circulation acts as a "thermospheric spoon" to mix the atmosphere. Since the circulation is stronger during solstice seasons because of the stronger difference in radiative forcing between the two hemispheres, it causes a global semiannual variation in neutral density with maxima during equinox seasons and minima during solstices. None of these can explain the annual term in density variation.

[8] The annual/semiannual variation also exists in the ionosphere. The annual/semiannual variation in ratio of atomic oxygen to molecular nitrogen O/N_2 has been considered as a cause of similar variation in N_mF_2, the peak electron density of F_2 layer [*Rishbeth and Müller-Wodarg*, 1999; *Rishbeth et al.*, 2000a, 2000b]. *Mendillo et al.* [2002] found that composition change is related to the seasonal variation in N_mF_2 but that temperature variation has a more significant influence on the F_2-layer height h_mF_2, and *Mendillo et al.* [2005] compared the annual (June/December) asymmetry in total electron content to O/N_2 asymmetry, identifying a possible relationship but finding that the ionospheric asymmetry is larger. *Rishbeth and Müller-Wodarg* [2006] further evaluated the annual asymmetry of N_mF_2, ruled out most of the known candidates, and concluded that some other processes, possibly due to lower atmosphere effects, must be implicated. Other efforts to explain neutral density variation in terms of lower atmospheric processes suggest changes in turbopause height [*Shimazaki*, 1971; *Chandra and Sinha*, 1974; *Schuchardt and Blum*, 1977]. Nevertheless, this mechanism remains speculative because of the lack of understanding of eddy diffusion at the mesopause and the effect of eddy diffusion on the thermosphere.

[9] The purpose of this study is to investigate mechanisms of seasonal variation in the upper atmosphere. The National Center for Atmospheric Research (NCAR) Thermosphere-Ionosphere-Electrodynamics General Circulation Model (TIE-GCM), satellite drag derived thermospheric neutral density data, and neutral composition data observed by the Global Ultraviolet Imager (GUVI) aboard the Thermosphere-Ionosphere-Mesosphere Energetics and Dynamics (TIMED) satellite were used for this study. The TIE-GCM solves the coupled thermosphere/ionosphere continuity, momentum, and energy equations self-consistently. It accounts for annual/semiannual forcing in the thermosphere and the ionosphere including the annual insolation variation, the semiannual "thermospheric spoon" effect, and the semiannual geomagnetic activity effect. However, through comparisons of model results to satellite drag data and neutral composition data, we found that the model produced much weaker annual/semiannual amplitude than observations, primarily because of lack of the July minimum in neutral density and composition. We thus examine lower atmospheric forcing that may drive the annual/semiannual variations in the thermosphere. Our basic hypothesis is that seasonal differences in gravity wave breaking cause systematic variation in eddy diffusion, which changes thermospheric composition by changing the rate at which atomic oxygen is removed from the lower thermosphere. Increased eddy diffusion reduces O/N_2, which in turn reduces neutral density throughout the thermosphere, because atomic oxygen declines with altitude much more slowly than molecular nitrogen because of its greater scale height. Section 2 introduces the NCAR

TIE-GCM. Section 3 describes the data used in this study, including the TIMED Solar EUV Experiment (SEE) data that were used as solar forcing for the TIE-GCM, the satellite drag-derived neutral density data, and the TIMED/GUVI composition data. Section 4 shows comparisons of the TIE-GCM simulations to observations of neutral density and composition that indicate much weaker annual/semi-annual amplitudes in the TIE-GCM simulations. Section 5 investigates effects of gravity-wave breaking induced circulation and eddy diffusivity on thermospheric composition, temperature, and neutral density. Section 6 gives evidence to support the idea that eddy diffusion is a plausible mechanism through which the lower atmosphere causes annual/semiannual variations in the thermosphere. Section 7 concludes this study and provides some discussion.

2. Model Description

[10] The TIE-GCM is a first-principle upper atmospheric general circulation model that solves the Eulerian continuity, momentum, and energy equations for the coupled thermosphere/ionosphere system. It utilizes a spherical coordinate system fixed with respect to the rotating Earth, with latitude and longitude as the horizontal coordinates and pressure surfaces as the vertical coordinate. The pressure interfaces are defined as $z = \ln(P_0/P)$, where P_0 is a reference pressure of 5×10^{-4} μb. The vertical range of the pressure interfaces is from -7 to 7, and thus covers altitude range about $97-600$ km depending on solar activity. The vertical resolution is 2 model grids per pressure scale height; the horizontal resolution is $5°$ latitude by $5°$ longitude, and the model time step is about 3 minutes. Output of the model are neutral, electron, and ion temperature; neutral and ion winds; concentrations of major species O, O_2, and N_2; concentrations of minor species $N(^4S)$, $N(^2D)$, NO; concentrations of ions $O^+, O_2^+, N_2^+, N^+,$ NO^+; electron density; and geopotential heights of pressure interfaces. Primary references for the NCAR upper atmospheric models include *Dickinson et al.* [1981, 1984], *Roble et al.* [1982, 1987, 1988], *Roble and Ridley* [1987, 1994], *Richmond et al.* [1992], *Roble* [1995], and *Richmond* [1995]. TIE-GCM v. 1.82 is used in this study.

[11] The external forcings of the TIE-GCM are solar irradiance, mainly in the extreme ultraviolet (EUV) and ultraviolet (UV) regions; geomagnetic energy input in the form of auroral energetic particle precipitation and ionospheric convection driven by the magnetosphere-ionosphere current system; perturbation at the lower boundary of the model by waves representing the interaction between the thermosphere/ionosphere system and lower atmosphere processes; and a specified upward or downward plasma flux at the upper boundary representing the interaction of the system with the plasmasphere. In this study, TIMED/SEE solar spectral irradiance measurements [*Woods et al.*, 2005] were used as solar input when available, and the EUVAC solar proxy model [*Richards et al.*, 1994] was used as solar input when the SEE measurements were not available. Ionospheric convection driven by the magnetosphere-ionosphere current system is specified by the empirical model of *Heelis et al.* [1982]. The auroral particle precipitation and its ionization and dissociation are calculated by an analytical auroral model described by *Roble and Ridley* [1987] but

updated to approximate the hemispheric power estimates of *Zhang and Paxton* [2008]. These magnetospheric energy inputs are scaled using the three-hour planetary K index (K_p). The migrating semi-diurnal and diurnal tides are specified at the lower boundary using the Global Scale Wave Model (GSWM) [*Hagan and Forbes*, 2002, 2003]. The effect of gravity wave breaking in the mesosphere-lower-thermosphere (MLT) region is included by specifying a constant eddy diffusivity at the lower boundary that declines with altitude. Effects of planetary waves and non-migrating tides are not considered.

3. Data

[12] Data used in this study include the TIMED/SEE solar spectral irradiance measurements, satellite drag derived neutral density data, and the TIMED/GUVI composition data.

[13] The TIMED/SEE measures solar spectral irradiance from $0.1-194$ nm [*Woods et al.*, 2005]. The TIMED satellite was launched on 7 December 2001, and normal operations began on 22 January 2002. The TIMED satellite has a circular polar orbit with altitude 630 km and an inclination of $74.1°$. The satellite circles the earth $15-16$ times a day and each orbit takes approximately 97 minutes. The SEE instruments measure solar spectral irradiance for three minutes per orbit. SEE consists of two channels: the EUV Grating Spectrograph (EGS) covers wavelengths from $27-194$ nm with a spectral resolution of 0.4 nm, and the X-ray Photometer System (XPS) component covers wavelengths from $0.1-34$ nm using broad-band photometers. The data used in this study are SEE version 8, level 3.

[14] The neutral density data used in this study are daily averaged neutral density at satellite perigee locations derived from five low-earth orbiting satellites, for 2002 to 2006. The five satellites are spherical objects with similar moderately eccentric orbits. The average perigee altitudes of the satellites are between 380 km and 430 km, and the average apogee altitudes are between 1300 km and 1650 km. The satellite perigees scan approximately three latitude cycles and five local time cycles in a year. The thermospheric neutral density at satellite perigees were calculated using a method developed by *Bowman et al.* [2004], with errors within $2-4\%$.

[15] Figure 1a shows the daily averaged neutral density at perigees for satellite #12388, from 2002 to 2006; Figure 1b is TIMED/SEE integrated ($5-105$ nm) solar EUV flux from day 2002039 to 2006365; and Figure 1c gives corresponding solar activity index $F_{10.7}$ index and geomagnetic A_p index. The density in Figure 1 is a composite of density variations with timescales from hours to decades and variations with geophysical locations due to variation in satellite perigee latitudes and altitudes. The density follows the overall morphology of the $F_{10.7}$ index and the TIMED/SEE observed solar flux, such as solar-rotational variation and solar-cycle variation. This indicates that solar irradiance is the main forcing of thermospheric neutral density. Accompanying the overall variation with solar irradiance are impulsive variations with geomagnetic forcing. This is evident by observing the spikes in density and the spikes of geomagnetic A_p index. Annual/semiannual density variation can be identified, with a minimum around July, a secondary
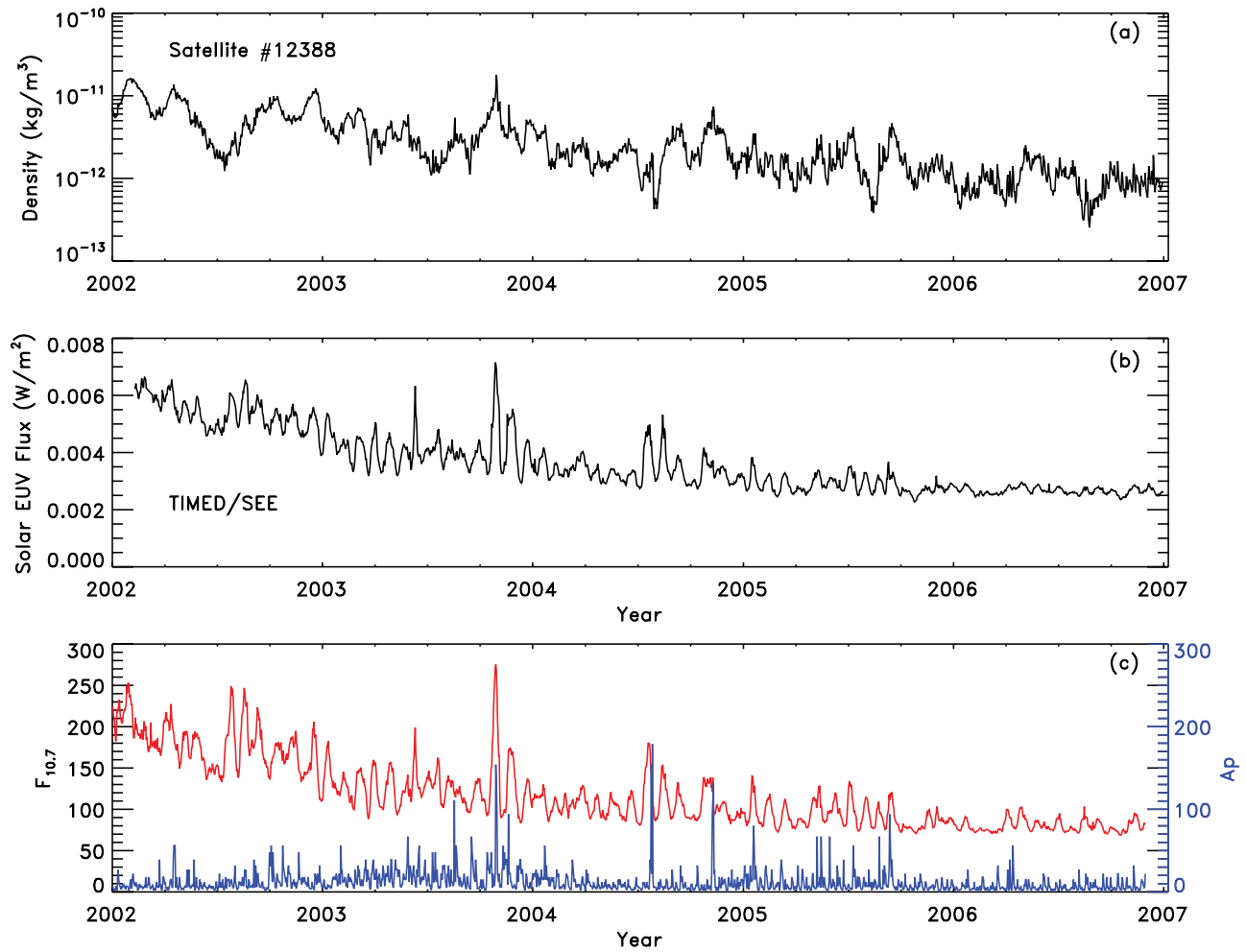
Figure 1. (a) Daily average neutral density at satellite perigee for satellite 12388 derived from atmospheric drag, from 2002 to 2006. (b) The TIMED/SEE integrated (5–105 nm) solar EUV flux from day 2002039 to 2006365. (c) Solar activity index $F_{10.7}$ and geomagnetic activity index A_p from 2002 to 2006.

minimum in January, and maximum near equinoxes. Other variations not evident but included in Figure 1a are the diurnal variation as perigee local time changes, latitudinal variation as perigee latitude varies between the southern hemisphere and the northern hemisphere, variation with height as perigee altitude varies between 385 km and 415 km because of the Earth's oblate shape. These variations make some contributions to the annual/semiannual variation shown in Figure 1. In addition, there is a global change due to increase of greenhouse gases [*Roble and Dickinson*, 1989; *Keating et al.*, 2000; *Emmert et al.*, 2004, 2008; *Marcos et al.*, 2005; *Qian et al.*, 2006] superimposed on the solar cycle variation of neutral density.

[16] The TIMED/GUVI measures the Earth's far ultraviolet (FUV) airglow in the spectral range from 120 to 180 nm [*Christensen et al.*, 2003]. It obtains images in five wavelength channels. These images are used to derive dayside composition, temperature, solar EUV flux, large-scale wave structure, and auroral processes. GUVI data are available from 2002 to present. In this study, we used GUVI disk measurements of column O/N$_2$, a level-3 product from the GUVI database. The sunlit disk emission measurements of two of the five channels, the atomic oxygen emission at 135.6 nm

(OI 135.6 nm) and N$_2$ LBH molecular bands (141 to 153 nm), are used to derive column number density ratio O/N$_2$ above an altitude where the N$_2$ column density is 10^{17} cm^{-2} (approximately 140 km) [*Strickland et al.*, 2004; *Zhang et al.*, 2004]. The locations corresponding to the GUVI measurements were selected from TIE-GCM model output, and the model column density ratios above the altitude where N$_2$ column number density is 10^{17} cm^{-2} were calculated and compared to the GUVI O/N$_2$.

4. Model Simulations of Density and Composition Variations

[17] TIE-GCM simulations of neutral density were compared to neutral density data derived from satellite drag data of five satellites to investigate numerical model capability in simulating neutral density and its variations. The TIE-GCM was run using TIMED/SEE measurements as solar input, from 2002 through 2006, except for the first 38 days of 2002, before SEE began routine operations, when EUVAC was used as solar input. The method described by *Solomon and Qian* [2005] was employed to calculate direct solar and photoelectron effects within the model. Daily averaged
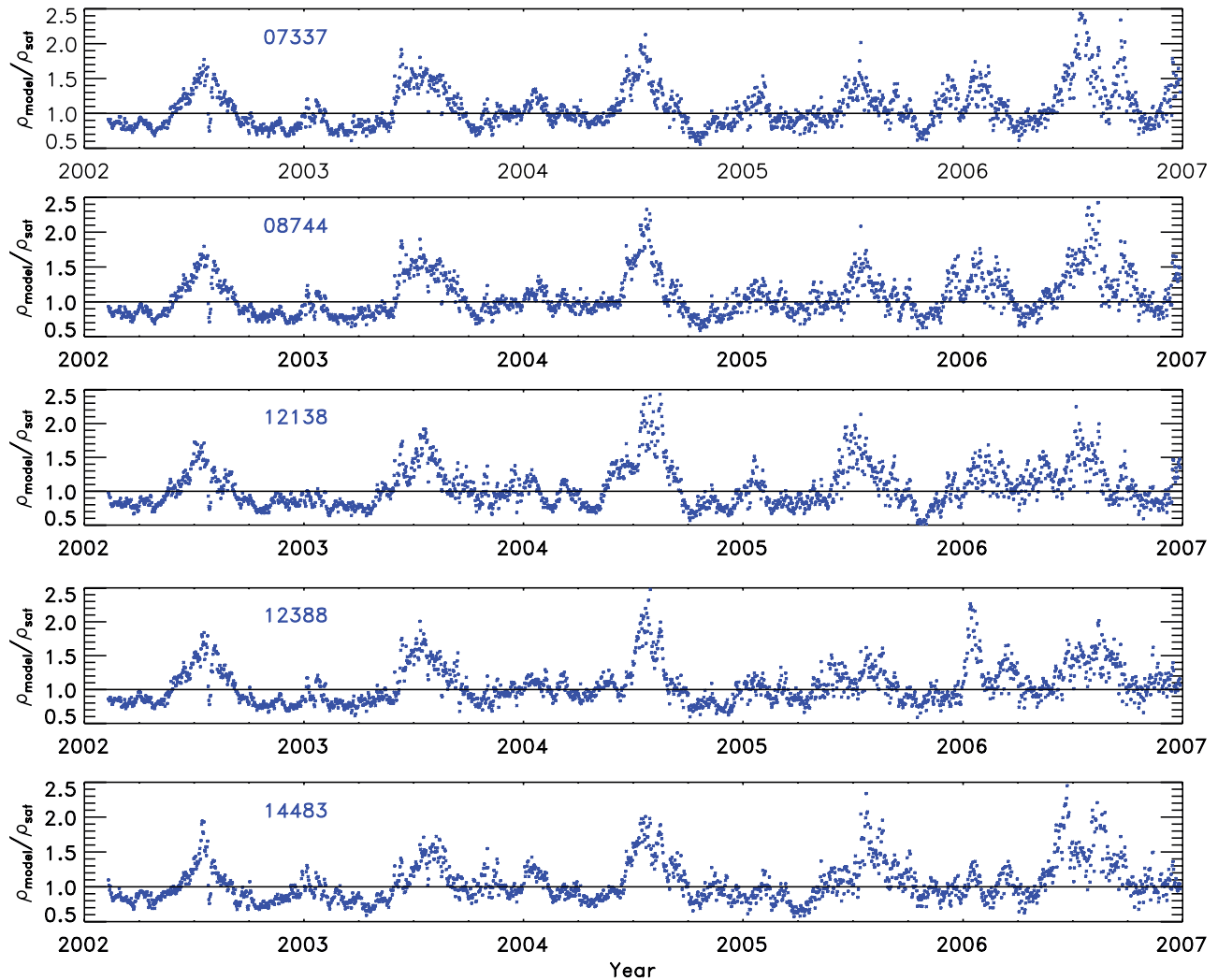
Figure 2. Strong seasonal pattern of discrepancy between model simulation and data: ratio of neutral density simulated by the TIE-GCM to satellite drag-derived neutral density for five satellites. The TIE-GCM model was run using TIMED/SEE measurements as solar input, assuming constant eddy diffusivity at the lower boundary (~97 km). Daily averaged neutral density of the TIE-GCM simulations was calculated at the perigee locations (altitude, latitude, and local solar time) of each satellite.

neutral density of the TIE-GCM simulations were calculated at perigee locations (altitude, latitude, and solar local time) of each satellite, and ratios of the TIE-GCM simulated density to satellite drag-derived density were calculated and shown in Figure 2 for all five satellites. The ratios in Figure 2 show a consistent seasonal pattern of disagreement between the model simulation and the data, especially during the July minimum period of neutral density. The model significantly overestimated the neutral density during this July minimum period and thus significantly underestimated the annual/semiannual amplitude observed by satellite drag data. This annual/semiannual pattern is true for all the five years and for all five satellites. Considering all the density variations embedded in Figure 1a, the pattern in Figure 2 suggests that the TIE-GCM model simulated important variations such as solar-cycle, solar-rotational, and geomagnetic variation very well, but did not replicate the seasonal variation.

[18] The lack of annual/semiannual amplitude in TIE-GCM simulations was further examined using TIMED/

GUVI composition data. Daily averaged column number density ratios O/N_2 were selected for the equatorial area (15°S to 15°N) and noon sector (10:30 am to 1:30 pm) from GUVI. The corresponding O/N_2 was also obtained for the TIE-GCM the same way as those for GUVI, i.e., referenced at altitude where N_2 column number density is 1×10^{17} cm^{-2} for each model point corresponding to satellite locations (latitude, solar local time) for each day. Figure 3 compares the column number density ratio for the GUVI and the TIE-GCM from 2002 to 2006. The GUVI O/N_2 has an annual/semiannual variation consistent with the annual/semiannual variation of satellite drag-derived neutral density, with minimum around July, a secondary minimum around January, and maximums during equinoxes. However, the annual/semiannual amplitude of TIE-GCM O/N_2 is also much weaker than that observed by GUVI, similar to the situation with model-data comparison of neutral density.

[19] It is necessary to examine the sources of the significant disagreement of seasonal variation between the model and
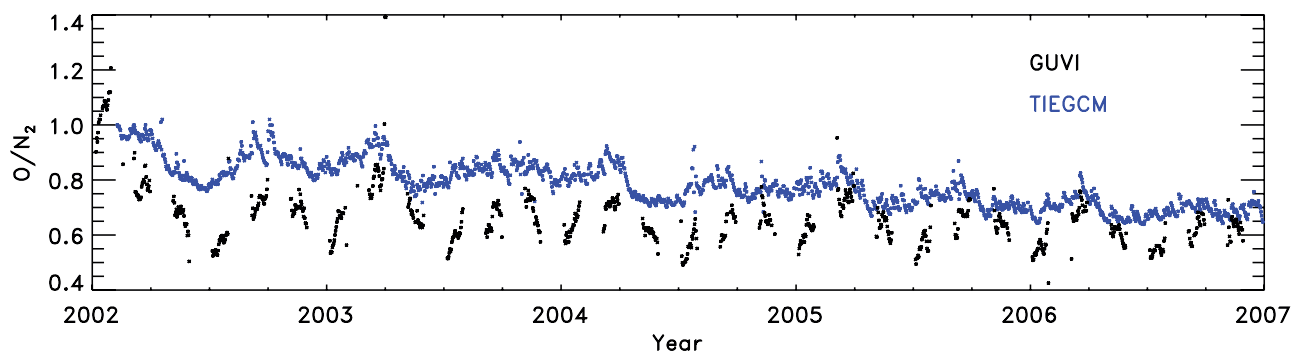
Figure 3. Column number density ratio O/N_2 above the altitude where the N_2 column number density is 10^{17} cm^{-2} (approximately 140 km). (black) TIMED/GUVI measurements; (blue) TIE-GCM simulation. The data were averaged over the equatorial region (15°S-15°N) and noon sector (10:30 am to 1:30 pm) whenever available in this location, and the model was sampled and averaged in the same way. The TIE-GCM model was run using TIMED/SEE measurements as solar input, assuming constant eddy diffusivity at the lower boundary (97 km).

the data. The TIE-GCM model solves upper atmospheric chemistry, dynamics, and electrodynamics self consistently. It does produce annual/semiannual variation in thermospheric parameters, for example, an annual variation due to annual insolation variation caused by the annual Sun-Earth distance variation and a global semiannual variation due to the "thermospheric spoon" effect [*Fuller-Rowell*, 1998]. Figure 4 shows TIE-GCM simulated global mean O/N_2, temperature, and neutral density at 400 km. In order to emphasize seasonal variation, the model was run under constant solar activity (solar maximum) and constant geomagnetic activity (geomagnetic quiet) conditions.

[20] Figure 4a shows the "thermospheric spoon" effect simulated by the TIE-GCM. Stronger mixing of the atmosphere during solstices causes less diffusive separation and smaller neutral density scale height, and thus lower neutral density. Near the equinoxes, the interhemisphere circulation is much weaker because solar heating is evenly distributed on the two hemispheres. Neutral species are more diffusively separated, and neutral density is larger because of larger scale height. A semiannual variation in O/N_2 is generated by the interhemispheric large circulation.

[21] The Earth's orbit has an eccentricity of 0.017. The Earth reaches its perihelion in early January, and passes through aphelion at the beginning of July. Because of the orbital eccentricity, the insolation is 7% larger in January than in July. Model sensitivity studies were conducted to investigate effect of the annual insolation variation on thermospheric parameters. Model sensitivity tests show that this 7% annual variation in solar irradiance can cause ~2% global mean temperature variation and ~20% global mean neutral density difference at 400 km. The annual amplitude of temperature shown in Figure 4b and the annual amplitude of neutral density shown in Figure 4c are consistent with model sensitivity test results. This shows that although the annual variation due to the Earth-Sun distance is captured realistically by the model, it is not sufficient to cause the observed density and composition effects.

[22] Despite the ability of the model to replicate known features of thermospheric variability, including solar and geomagnetic forcing, Earth-orbital effects, and internal dynamic processes, the TIE-GCM simulations do not fully

account for the seasonal amplitudes, as shown in comparisons to satellite drag data (Figure 2) and the TIMED/GUVI composition data (Figure 3). This suggests a need for additional annual/semiannual forcing. In the next section, propagation of gravity waves, generated in the lower atmosphere, through the middle atmosphere, resulting in changes in eddy mixing in the mesopause region, will be explored
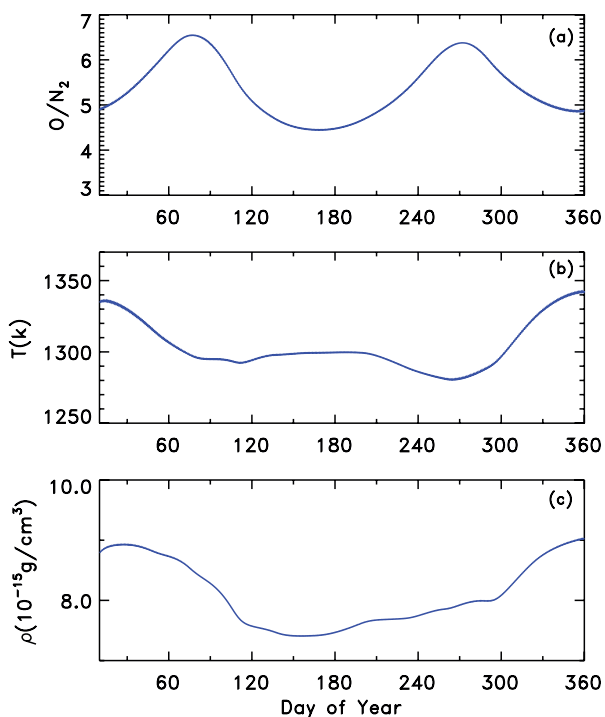

Figure 4. Global mean O/N_2, neutral temperature, and neutral density at 400 km under solar maximum and geomagnetic quiet conditions simulated by the TIE-GCM. A significant semiannual variation is seen in composition, and there is an annual variation in temperature due to variation of the Sun-Earth distance, but the net effect on density results in both semiannual and annual variation much smaller than observed.
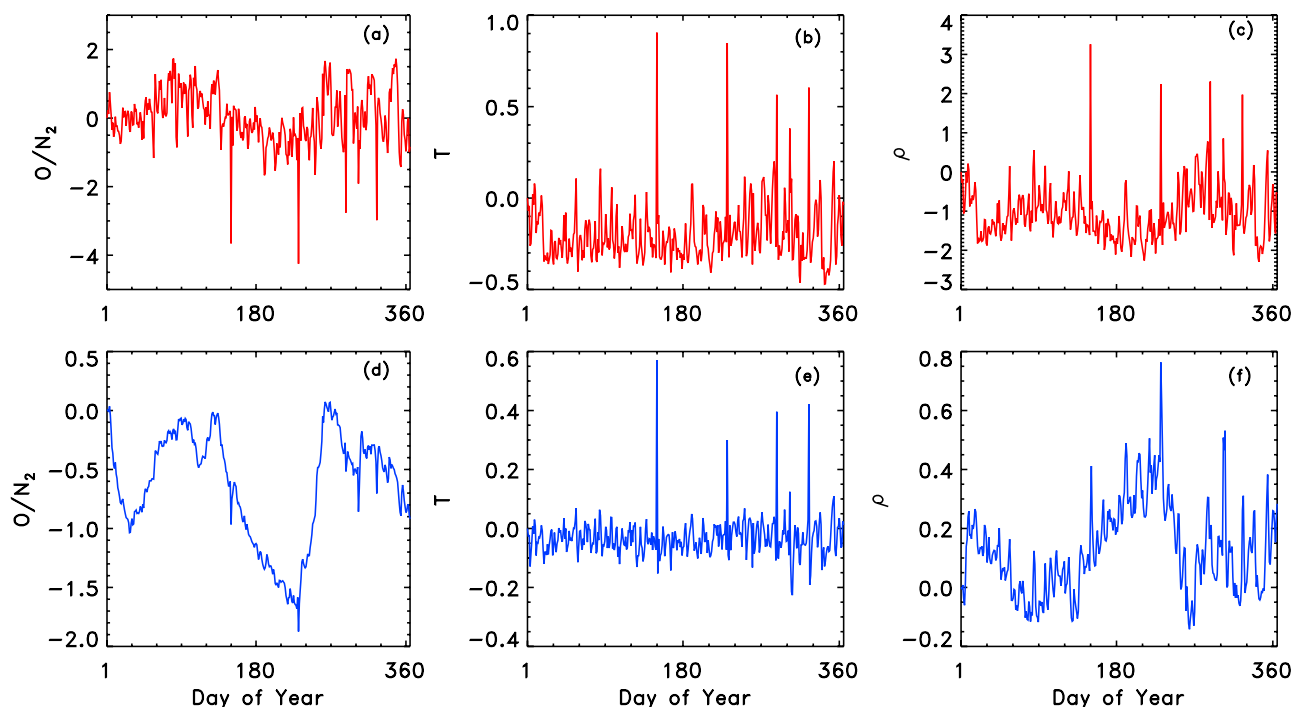
Figure 5. Simulated percentage difference in global-averaged thermospheric temperature, composition, and density generated by gravity wave momentum deposition in the mesopause region for 2003. (a, b, and c in red) At 400 km; (d, e, and f in blue) at 120 km.

as an additional mechanism of seasonal variation in the thermosphere.

5. Seasonal Variation in Lower Atmosphere Forcing

[23] The TIE-GCM has a lower boundary at the pressure interface $\ln(P_0/P) = -7$, which is at about 97 km. This is a region where waves and tides strongly affect atmospheric dynamics and energetics. The TIE-GCM includes tidal effects using the GSWM [*Hagan and Forbes*, 2002, 2003]. Effects of planetary waves are not considered since most planetary waves dissipate in the middle atmosphere, below the altitude range of the TIE-GCM. Effects of turbulent mixing, primarily caused by gravity wave breaking, are included using an eddy diffusion coefficient that is constant with respect to season, solar time, and location, although it does decrease with altitude (see section 5.2).

[24] Gravity wave breaking in the MLT region deposits momentum and produces small-scale turbulence [e.g., *Hodges*, 1969; *Hines*, 1970; *Lindzen*, 1971; *Fritts*, 1984; *Garcia and Solomon*, 1985; *Akmaev*, 2001a, 2001b]. It has been suggested that gravity wave breaking exhibits strong seasonal variation [*Garcia and Solomon*, 1985; *Akmaev*, 2001a, 2001b]. In this section, the effects of the seasonal variation of gravity wave breaking on annual/semiannual variations in the thermosphere will be investigated.

5.1. Circulation Induced by Gravity Waves

[25] A candidate for inducing seasonal variation in the thermosphere is changes in circulation induced by gravity wave acceleration. Zonal acceleration deposited by gravity wave drag is eastward in the summer hemisphere and

westward in the winter hemisphere. Under Coriolis force, the opposite direction of the wind acceleration in the two hemispheres during solstice seasons causes interhemisphere flow from the summer hemisphere to the winter hemisphere. During equinox seasons, the wind acceleration from gravity waves is much smaller and there is no distinct difference in direction between the two hemispheres. This results in a seasonal variation in vertical motion, which in turn could affect thermospheric composition. This seasonal wind acceleration pattern was imposed as a momentum source at the lower boundary of the TIE-GCM, in order to investigate the magnitude of the possible effects.

[26] To estimate these global circulation effects, calculations of zonal acceleration were obtained from the extended version of the TIE-GCM, the Thermosphere-Ionosphere-Mesosphere-Electrodynamics General Circulation Model (TIME-GCM) [*Roble and Ridley*, 1994]. This model includes a gravity wave parameterization scheme based on the work of *Lindzen* [1981]. Zonal acceleration calculated by the TIME-GCM was added to the zonal momentum equation at the lower boundary of the TIE-GCM and the changes in global-averaged thermospheric composition, temperature, and density caused by this additional momentum source were calculated. Figure 5 shows the percentage differences at 400 km and 120 km during 2003. Thermospheric mixing is increased by the induced vertical motion during the solstices, which decreases O density and increases N_2. Consequently, the O/N_2 ratio exhibits an annual/semiannual variation, which causes a similar change in neutral density at 400 km. However, although the morphology of the seasonal variation is similar to the observational evidence, the magnitude is far too small to account for its amplitude. This indicates that seasonal effects on gravity wave generation,
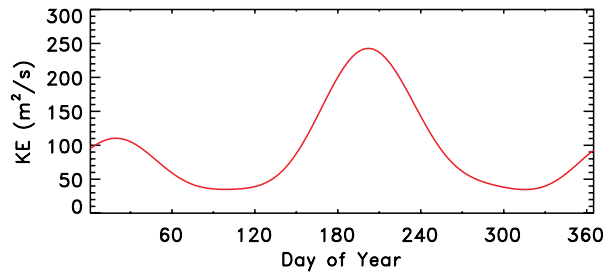
Figure 6. Variation of the eddy diffusion coefficient applied at the lower boundary of the TIE-GCM ($\sim$97 km). The unit of eddy diffusion coefficients used in the TIE-GCM and in equations (1) and (2) is s^{-1}. Eddy diffusion coefficients in unit of s^{-1} were multiplied by the square of scale height to be transferred to units of m^2/s, assuming a scale height of 5 km at the TIE-GCM lower boundary.

filtering, and energy/momentum deposition may be implicated, but that a different mechanism accounts for thermospheric effects.

5.2. Eddy Diffusion

[27] Gravity wave breaking in the MLT region produces small-scale turbulence, and gravity wave energy is dissipated into heat through eddy diffusion [*Hodges*, 1969]. Other tidal and wave activity can also contribute to eddy diffusion in the mesopause region. For example, diurnal tides can break down in the MLT region and generate turbulence [*Lindzen*, 1967]. Regardless of the sources, both ground-based and satellite observations indicate that eddy diffusion in the mesopause region exhibits strong seasonal variation [*Kirchhoff and Clemesha*, 1983; *Fukao et al.*, 1994; *Lübken*, 1997; *Khattatov et al.*, 1997; *Rao et al.*, 2001; *Sasi and Vijayan*, 2001]. Eddy diffusion is larger during the solstices than the equinoxes, with stronger turbulence in summer than in winter. The difference can be as large as one order of magnitude. Efforts to model seasonal variations in eddy diffusion [*Blum and Schuchardt*, 1978; *Garcia and Solomon*, 1985; *Akmaev*, 2001b] show good agreement with observations.

[28] Furthermore, it appears that the seasonal variation of eddy diffusion in the MLT is largely a global phenomenon. *Fukao et al.* [1994] derived a seasonal variation of approximately one order of magnitude, with maximum in the summer and minima at the equinoxes, from radar measurements at 35°N. *Kirchhoff and Clemesha* [1983] obtained a minimum eddy diffusion coefficient of 45 m^2/s during fall and a maximum of 123 m^2/s during summer based on radar measurements at 23°S. *Sasi and Vijayan* [2001] analyzed Doppler radar data over a station at 13.5°N and found that eddy diffusion varies from $\sim$25–300 m^2/s during September and June, and such seasonal variation is not significantly different at different latitudes. *Lübken* [1997] investigated turbulent properties in the MLT region using sounding rocket data over 68°N and 69°N and found that the maximum eddy diffusion coefficient in the upper mesosphere is

183 m^2/s in the summer and 100 m^2/s in the winter. *Garcia and Solomon* [1985] found an eddy diffusion coefficient of $\sim$300 m^2/s in the summer, $\sim$100 m^2/s for the winter, and $\sim$50 m^2/s during equinoxes at 61°N in the height range of 80 km to 100 km, and *Khattatov et al.* [1997] also found that the magnitudes of the eddy diffusion coefficients at middle latitude ranges from 50 up to 300 m^2/s in the region 80−100 km.

[29] Sensitivity studies were conducted to investigate the effect of eddy diffusion on thermospheric neutral density. For example, TIE-GCM simulations showed that an increase in the eddy diffusion coefficient at the model lower boundary by a factor of two causes a 20% decrease in neutral density at 400 km, with an e-folding time of this density change on the order of 10 days. An annual/semiannual variation of eddy diffusion was derived by fitting these sensitivity test results to the satellite drag data residuals for the five satellites and five years shown in Figure 2 (2002−2006). The eddy diffusion coefficient at the lower boundary was represented as a Fourier series with four harmonics per year, as follows

$$K_E(\omega) = A_1 + A_2 \sin(\omega) + A_3 \cos(\omega) + A_4 \sin(2\omega) + A_5 \cos(2\omega)$$
$$+ A_6 \sin(3\omega) + A_7 \cos(3\omega) + A_8 \sin(4\omega) + A_9 \cos(4\omega)$$
$$(1)$$

where $K_E(\omega)$ is in units of s^{-1}, $\omega = 2\pi\theta$, $\theta = (\text{day-1})/365$, and $A_1 - A_9$ are coefficients obtained from the model fit. Above the lower boundary, the eddy diffusivity is assumed to decrease exponentially with increasing height

$$K_E(\omega, z) = K_E(\omega) \times e^{(-7-z)} \qquad (2)$$

where z represents the TIE-GCM pressure coordinate $z = \ln(P_0/P)$. Table 1 lists the coefficients for equation (1), and Figure 6 shows the resulting estimate of the eddy diffusion coefficient $K_E(\omega)$ as a function of day of the year, in units of m^2/s, assuming a scale height of 5 km at the TIE-GCM lower boundary. This curve exhibits an annual/semiannual variation comparable to those of *Garcia and Solomon* [1985], *Khattatov et al.* [1997], and others. Since gravity wave breaking is considered to be a major source of eddy diffusivity in the mesopause region, we hypothesize that the Ke obtained from data fitting could represent the effect of turbulent mixing mainly caused by gravity wave breaking. The eddy diffusion coefficient shown in Figure 6 is imposed at the lower boundary of the TIE-GCM globally, with no variation in latitude, longitude, or solar time.

[30] Figure 7 plots percentage differences between the standard TIE-GCM and the modified version described above, during 2003. The changes in global-averaged thermospheric composition, temperature, and density at 120 km and 400 km are shown. Since eddy diffusion in the lower thermosphere transports O downward and O_2 and N_2 upward, at 120 km, the large eddy diffusivity in the northern hemisphere summer decreases the O number density. Eddy

Table 1. Fourier Coefficients for Annual/Semiannual Variation of Eddy Diffusion (s^{-1})

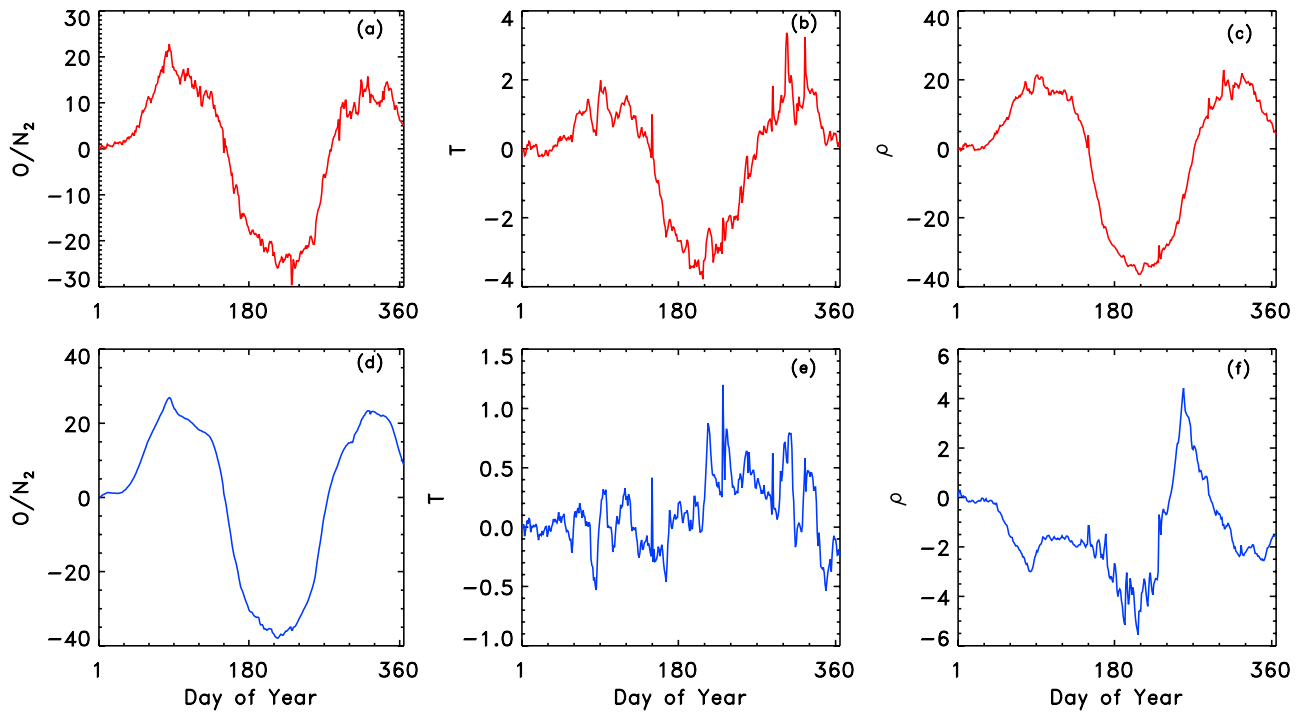| A_1	A_2	A_3	A_4	A_5	A_6	A_7	A_8	A_9
4.06×10^{-6}	-8.77×10^{-7}	-2.28×10^{-6}	1.77×10^{-6}	2.15×10^{-6}	-3.05×10^{-7}	-2.66×10^{-7}	4.08×10^{-7}	1.59×10^{-7}

Figure 7. Simulated percentage difference in global-averaged thermospheric temperature, composition, and density introduced by application of the variation in eddy diffusion shown in Figure 6 to the TIE-GCM lower boundary (∼97 km) during 2003. (a, b, and c in red) At 400 km; (d, e, and f, in blue) at 120 km.
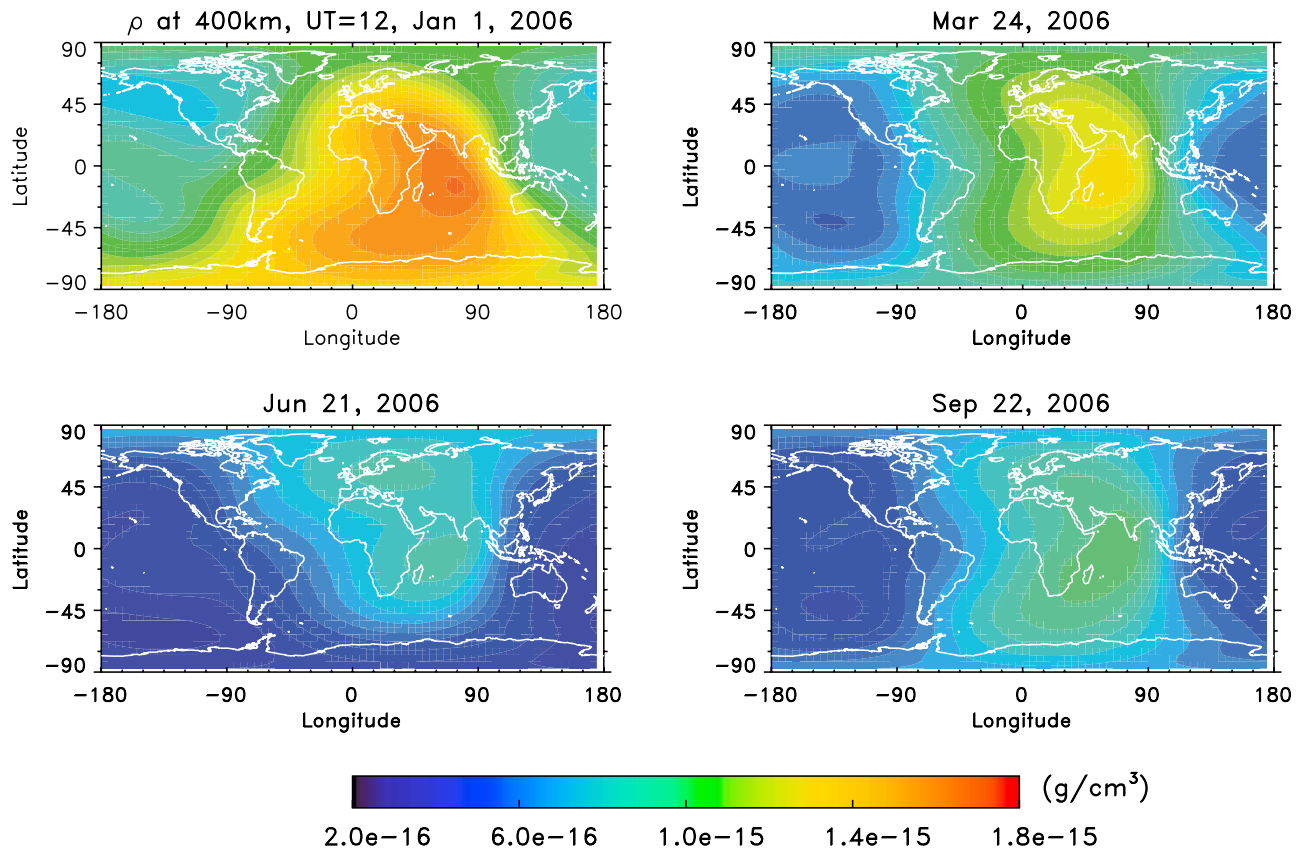

Figure 8. Neutral density at 400 km simulated by the TIE-GCM at noon universal time for 4 days, representative of solstice and equinox conditions, during geomagnetically quiet times and low solar activity. Seasonal variation of the lower-boundary eddy diffusion coefficient as shown in Figure 6 was applied.
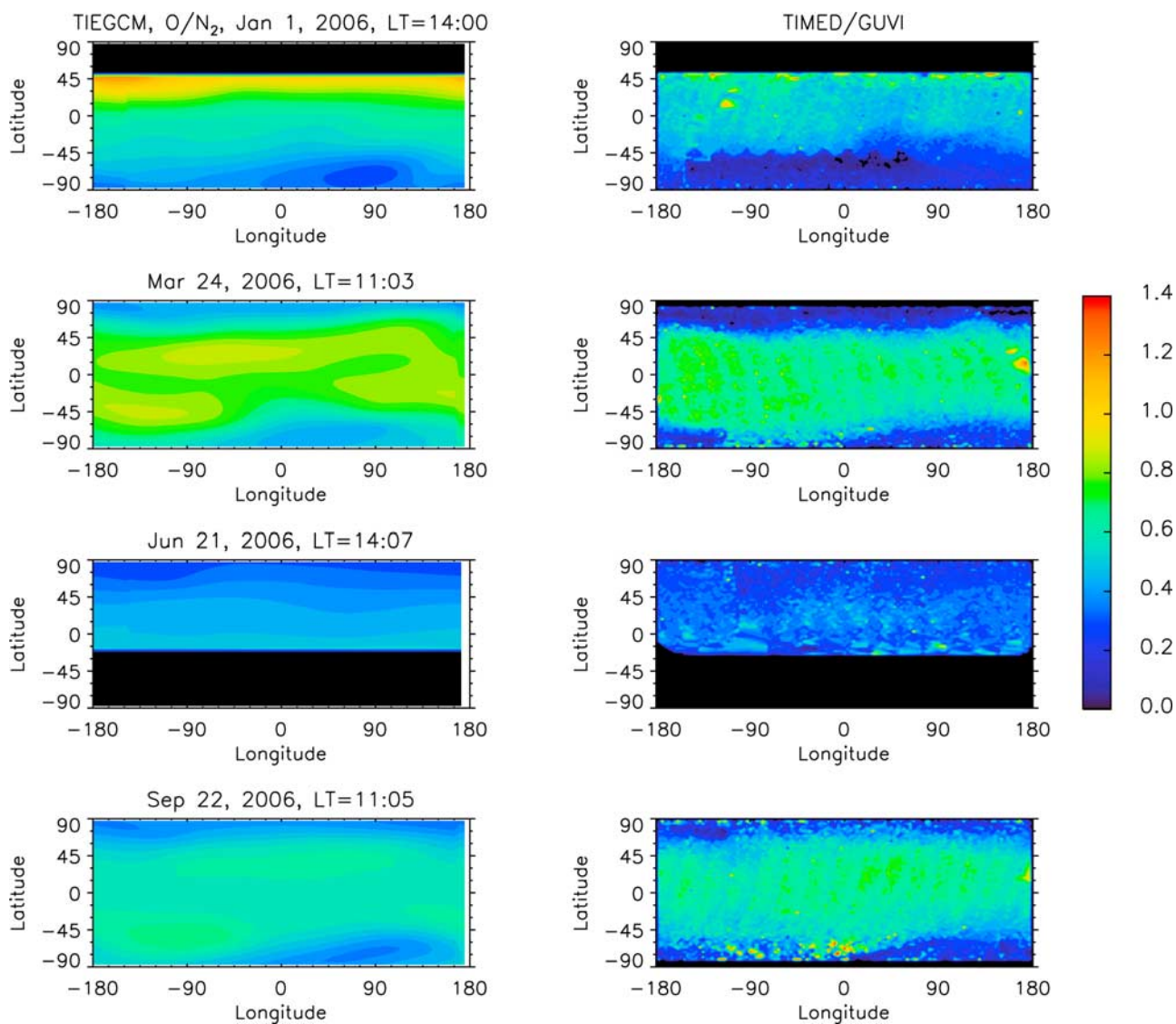
Figure 9. Atomic oxygen to molecular nitrogen (O/N$_2$) column density ratio during the same 4 days as shown in Figure 8, representative of solstice and equinox conditions. (left) TIE-GCM simulation. The longitudes in these plots are sampled at constant local time to approximate the satellite observational pattern. (right) GUVI observations.

diffusion has a much smaller effect on N$_2$ because it is the primary atmospheric constituent at these altitudes. This change in atomic and molecular constituents is partially modified by change in O$_2$ loss through photodissociation and change in O recombination. The reduction in O number density at 120 km propagates to the upper thermosphere through molecular diffusion, and is seen in the model results at 400 km. The percentage difference in the ratio of O/N$_2$ shows an annual/semiannual variation that is consistent with the effect of eddy diffusivity on O and N$_2$.

[31] The percentage difference in temperature is small at 120 km, but increases with altitude. Increase in eddy diffusivity reduces O/N$_2$ and density, which in turn reduces solar heating. Other factors contribute to decreased temperatures. The increase of NO due to decreased O/O$_2$ ratio causes increased NO infrared cooling, and increased eddy diffusion increases cooling by downward eddy transport of heat. This is partially offset by a decrease in the thermal conductivity coefficient. The combined effects from solar heating, NO cooling, eddy conduction, and thermal conduction result in a small decrease in temperature for increased eddy diffusivity.

[32] Figure 7c shows that the combined effect of reduction in O density and thermal contraction causes a density decrease at 400 km of nearly 40% during the northern hemisphere summer and an increase about 20% during the equinox seasons. The change in composition is the largest contribution to this reduction. The amplitude in percentage difference of neutral density increases with altitude due to the cumulative effect of the reduction in mean atmospheric scale height.

[33] These simulations reveal a new finding that eddy diffusion can influence thermospheric composition, and hence neutral density, more strongly than the large-scale circulation. Locally, the effect of dynamic forcing on composition is compensated for by thermal forcing in influencing
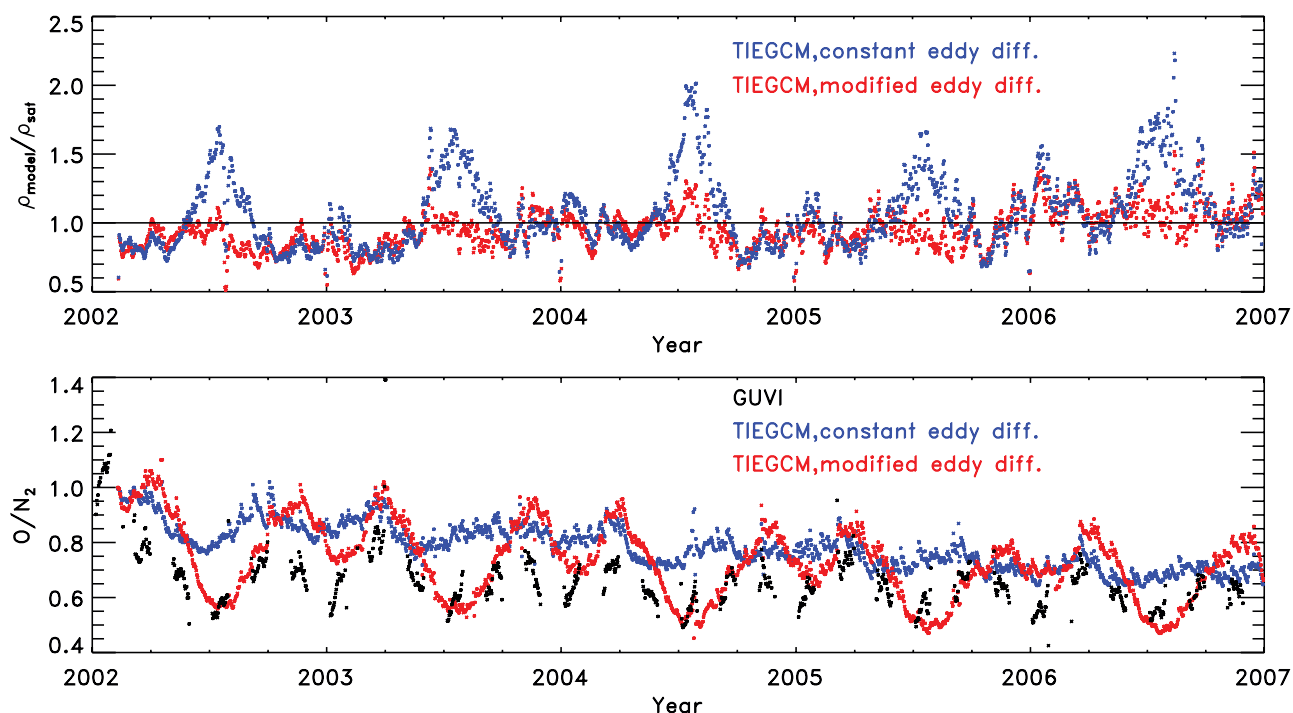
Figure 10. (top) Ratios of neutral density simulated by the TIE-GCM to satellite drag measurements. The average density ratio for the five satellites (see Figure 2) is plotted. (blue) TIE-GCM simulation using constant eddy diffusion at the lower boundary. (red) TIE-GCM simulation using the variation of eddy diffusion at the lower boundary shown in Figure 6. (bottom) Column number density ratio O/N_2 as described in Figure 3. (black) TIMED/GUVI measurements; (blue) TIE-GCM simulation using constant eddy diffusion at the lower boundary; (red) TIE-GCM simulation using the variation of eddy diffusion at the lower boundary shown in Figure 6.

neutral density—upwelling associated with heating results in reduced O/N_2. Globally, the large-scale circulation transports energy and mass between the summer hemisphere and the winter hemisphere and result in large latitude dependence in temperature and O/N_2. However, much of the effect on neutral density is canceled in the global mean sense: areas of upwelling compensate for areas of downwelling. Unlike the large-scale circulation, the effect of eddy diffusion on temperature compounds the effect of eddy diffusion on composition in changing neutral density as increased eddy diffusivity reduces both O/N_2 and temperature, and thus neutral density.

6. Results

[34] TIE-GCM simulations using the modified eddy diffusion coefficient shown in Figure 6 were compared to satellite drag data and to TIMED/GUVI composition data. Example global density maps representative of these simulations are shown in Figure 8 for 4 days during 2006, representative of the two solstice periods and the two equinox periods. 2006 was a fairly quiet year near solar minimum, and there was no significant geomagnetic activity during the three days prior to and including the example days, so that the seasonal effects are isolated. The solstice-to-equinox change in overall density and its morphology is clear, as is the large difference between southern summer solstice and northern summer solstice. In Figure 9, a comparison between the model simulation of O/N_2 column density and data from

TIMED/GUVI is shown for these same 4 days. In this case, the model is sampled at constant local solar time over the course of the day, so as to approximate the satellite observational pattern. GUVI performs this measurement over sunlit, non-auroral regions, so the latitude sampling is incomplete, but the comparison for the latitudes shown at the selected solar times is reasonable.

[35] Figure 10a shows the ratios of the TIE-GCM neutral density to satellite drag derived density. The ratios are average ratio for the five satellites. The results demonstrate consistent improvement in annual/semiannual density variation, especially during the July minima, for all the years. Figure 10b compares TIE-GCM O/N_2 to TIMED/GUVI O/N_2 measurements in the same manner as Figure 3. Imposition of an annual/semiannual variation of eddy diffusion causes the TIE-GCM O/N_2 to exhibit an annual/semiannual pattern that is more consistent with TIMED/GUVI observation, similar to the case for the neutral density. Since the satellite drag measurements were used to derive annual variation of the eddy diffusion coefficient, the improvement in agreement with density is expected; the similar improvement with composition measurements implies support for this adjustment, and support for the suggestion that composition change is the primary mechanism.

[36] Some discrepancies remain between model simulations and observations. The annual eddy diffusion function employed is constant from year to year, representing essentially an annual average, but there are clearly interannual variations in the data. The observed O/N_2 has a strong
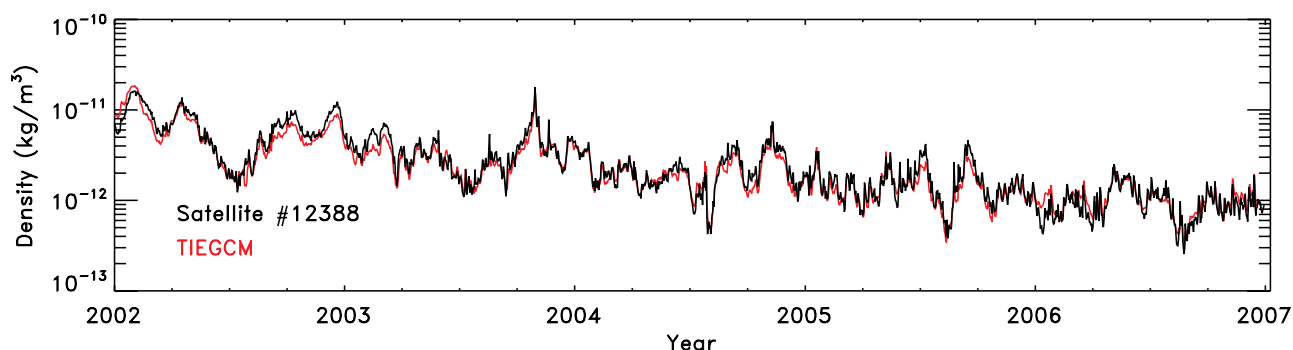
Figure 11. Data-model comparison of thermospheric neutral density at satellite perigees for satellite 12388 from 2002 to 2006. (black) Satellite drag derived density, same as Figure 1a; (red) TIE-GCM simulation. The TIE-GCM was run using TIMED/SEE measurements as solar input, with the annual/ semiannual variation of eddy diffusivity (Figure 6) imposed at the lower boundary (~97 km).

semiannual variation but the annual term does not appear to be as significant as in the model. Since a globally uniform eddy diffusivity was employed at the model lower boundary, latitudinal and solar time effects may be underestimated.

[37] Figure 11 shows the TIE-GCM simulated neutral density and satellite drag derived neutral density for satellite #12388 for the years 2002-2006. The EUVAC solar proxy model [*Richards et al.*, 1994] was used as solar input for the first 38 days of 2002 and SEE data were used from day 39 of 2002, through 2006. The TIE-GCM simulation with modified eddy diffusion coefficient obtains very good agreement with neutral densities derived from all five satellites, on timescales spanning solar cycle, seasonal, solar rotational, and even daily changes driven primarily by geomagnetic events.

7. Discussion

[38] This study demonstrates the influence of lower and middle atmosphere processes on thermospheric density. By process of elimination, the large differences observed between the two solstices must be due to the lower atmosphere: change in the Sun-Earth distance is too small to account for the variation; geomagnetic activity is insufficiently variable, and other known asymmetries between the hemispheres, such as the offset of the magnetic field, are inconsequential, particularly at solar minimum. Analogous to the discussion of ionospheric asymmetry by *Rishbeth and Müller-Wodarg* [2006], we can easily rule out galactic, interplanetary, magnetospheric, and plasmaspheric causes, but note their speculation that perhaps the explanation could be "hemispheric differences in weather and climate in the lower atmosphere". Seasonal/hemispheric differences in the troposphere, driven by differences in land mass distribution, circulation, convection, and frontal activity, are well known. These also cause differences in the dynamics of the stratosphere and mesosphere through mechanisms controlled largely by gravity wave acceleration, drag, and filtering. Therefore it is not surprising that these effects are evidently manifested in the thermosphere as well. The question is, what are the mechanisms?

[39] The chain of causation proposed here is as follows: Gravity wave breaking causes changes in eddy mixing, as parameterized by the eddy diffusion coefficient. This causes

change in lower thermosphere composition as increased eddy diffusion accelerates the downward transport of atomic oxygen to the mesopause, where it recombines into molecular oxygen. Composition change in the lower thermosphere is transmitted throughout the thermosphere through molecular diffusion, and the difference in scale height between O and N_2 means that if the O/N_2 ratio decreases, upper thermosphere density also decreases. Observations by TIMED/ GUVI support the proposition that composition change is the primary cause of density change. This is also seen in mass spectrometer data, as captured by the MSIS series of empirical models.

[40] This is not the only possible explanation for the observed variation. The imposition of an empirical variation in the eddy diffusion coefficient is an ad-hoc solution that exploits the most effective way, in the model, to change composition. The density and composition observations support the fact of the composition change, but not necessarily the mechanism. We have used seasonal variation of eddy diffusivity to generate this composition change; however, other lower atmospheric processes may also contribute to the composition change as discussed in the following paragraphs. Furthermore, we have adopted a simplified approach by changing the eddy diffusion coefficient with day of the year, but keeping it constant with location. This results in good agreement with density data but an imperfect match with the annual portion of the composition variation. Additionally, this approach cannot describe interannual variability, which is evident in the density data ratios shown in Figure 2. However, another striking aspect of Figure 2 is the similarity among the time series for all satellites, despite the different sampling caused by their evolving perigee locations. For instance, 2003 has a very different shape than 2002, but each satellite describes a very similar seasonal variation for the respective years. This implies that whatever the sources of the seasonal variation, by the time it reaches the upper thermosphere, it is essentially a global phenomenon. There is observational support for the global nature of variations in eddy diffusivity, as discussed in section 5.2.

[41] Additional candidates for propagation of variable lower-atmosphere effects to the thermosphere are atmospheric tidal oscillations. Migrating diurnal and semi-diurnal tides are included in the TIE-GCM through empirical specification by the GSWM at the lower boundary, including seasonal

changes. However, non-migrating tides are not included, and as these are now implicated in ionospheric morphology [e.g., *Immel et al.*, 2006], and are known to vary seasonally, they could be considered a candidate. This work does not exclude a contribution from this source, although it is not likely that mixing sufficient to cause the large changes in composition could be accomplished by tidal variation alone.

[42] The annual oscillation (AO) and semiannual oscillation (SAO) in mesospheric wind and temperature [e.g., *Hirota*, 1980; *Remsberg et al.*, 2002; *Huang et al.*, 2006] could also play a role in thermospheric modulation. Dynamical processes such as wave-mean flow interaction and wave-wave interactions, including gravity waves and planetary waves, have been invoked as mechanisms [e.g., *Lindzen*, 1981; *Dunkerton*, 1982; *Hitchman and Leovy*, 1986]. The AO and SAO are signatures of annual/semiannual variation of gravity wave breaking in the MLT region, and thus could either be diagnostic of thermospheric processes or play a role in gravity wave filtering. Planetary waves that drive equatorial oscillations in the stratosphere are largely dissipated there and therefore less likely to significantly affect the dynamics of the upper mesosphere. However, it is an intriguing observation that there appears to be a two-year periodicity in the interannual variability seen in Figure 2, with even-numbered years having a larger and sharper July minimum in observed density. These years are coincident with the eastward phase of the quasi-biennial oscillation (QBO). We draw no conclusions from this limited sample, but note that other thermospheric effects have also been tied to the QBO [e.g., *Wu et al.*, 2008].

[43] The TIE-GCM in its standard configuration, when driven using measured solar irradiances, does an excellent job in reproducing the densities forced on by solar cycle, solar rotational, and geomagnetic variation. This lends considerable confidence to the result, and points to a missing source of seasonal variation rather than some shortcoming of model physics. The general circulation of the thermosphere appears to be adequately described by the TIE-GCM, and the semiannual variation in composition described by *Fuller-Rowell* [1998] as the "thermospheric spoon" is replicated by the model. This work does not contradict, but rather confirms, the semiannual effects described by Fuller-Rowell. However, the "thermospheric spoon" cannot explain the differences between the solstices, the semiannual amplitude is not as large as observed in the GUVI data, and the effect on density is small, at least in our model. Therefore the general circulation of the thermosphere can only be part of the solution, and lower atmosphere effects must provide the rest.

[44] The next steps in understanding the interactions between lower and upper atmosphere are to perform full simulations of atmospheric processes that couple wave, tidal, and dynamical processes from the surface to the exobase, for example, using the Whole Atmosphere Community Climate Model [*Marsh et al.*, 2007]. This approach can capture generation of all tidal modes, interannual variability, and even day-to-day variability, but is still dependant on a gravity wave parameterization scheme. A methodology that includes orographic, convective, and frontal generation of gravity waves, acceleration of and filtering by middle atmospheric jets, and eddy mixing through their breaking, could possibly describe the observed thermospheric variation. However, observational constraints on mesospheric general circulation already places strong constraints on gravity wave processes, and it remains to be seen whether parameterizations that capture middle-atmosphere dynamics can also characterize thermospheric variation. Another approach may be observation of mixing variation itself through analysis of CO_2 profiles such as measured by the SABER instrument on TIMED. A combination of modeling and observational approaches should advance the understanding of seasonal processes in the upper atmosphere, which in turn could hold the key to a full quantification of short-term variability as well.

References

Akmaev, R. A. (2001a), Simulation of large-scale dynamics in the mesosphere and lower thermosphere with the Doppler-spread parameterization of gravity waves: 1. Implementation and zonal mean climatologies, *J. Geophys. Res.*, *106*, 1193–1204.

Akmaev, R. A. (2001b), Simulation of large-scale dynamics in the mesosphere and lower thermosphere with the Doppler-spread parameterization of gravity waves: 2. Eddy mixing and the diurnal tide, *J. Geophys. Res.*, *106*, 1205–1213.

Blum, P. W., and K. G. H. Schuchardt (1978), Semi-theoretical global models of the eddy diffusion coefficient based on satellite data, *J. Atmos. Terr. Phys.*, *40*, 1137–1142.

Bowman, B. R. (2004), The semiannual thermosphere density variation from 1970 to 2002 between 200–1100 km, AAS 2004-174, paper presented at the AAS/AIAA Spaceflight Mechanics Meeting, Maui, Hawaii, 8–12 February.

Bowman, B. R., F. A. Marcos, M. Kendra (2004), A method for computing accurate daily atmospheric density values from satellite drag data, AAS 2004-173, paper presented at the AAS/AIAA Spaceflight Mechanics Meeting, Maui, Hawaii, 8–12 February.

Chandra, S., and A. K. Sinha (1974), The role of eddy turbulence in the development of self-consistent models of the lower and upper thermosphere, *J. Geophys. Res.*, *79*, 1916–1922.

Christensen, A. B., et al. (2003), Initial observations with the Global Ultraviolet Imager (GUVI) in the NASA TIMED satellite mission, *J. Geophys. Res.*, *108*(A12), 1451, doi:10.1029/2003JA009918.

Cook, G. E. (1967), The large semiannual variation in exospheric density: A possible explanation, *Planet. Space Sci.*, *15*, 627–632.

Cook, G. E. (1969), The semiannual variation in the upper atmosphere: A review, *Ann. Geophys.*, *25*, 451–469.

Detman, T. R. (1996), Cross validation comparisons of autonomous Ap predictions, in *Proceedings of Workshop on the Evaluation of Space Weather Forecasts*, edited by K. Doggett, 149 pp., NOAA, ERL, Boulder, Colo.

Dickinson, R. E., E. C. Ridley, and R. G. Roble (1981), A three-dimensional general circulation model of the thermosphere, *J. Geophys. Res.*, *86*, 1499–1512.

Dickinson, R. E., E. C. Ridley, and R. G. Roble (1984), Thermospheric general circulation with coupled dynamics and composition, *J. Atmos. Sci.*, *41*, 205–219.

Dunkerton, T. J. (1982), Theory of the mesopause semiannual oscillation, *J. Atmos. Sci.*, *39*, 2681–2690.

Emmert, J. T., J. M. Picone, J. L. Lean, and S. H. Knowles (2004), Global change in the thermosphere: Compelling evidence of a secular decrease in density, *J. Geophys. Res.*, *109*, A02301, doi:10.1029/2003JA010176.

Emmert, J. T., J. M. Picone, and R. R. Meier (2008), Thermospheric global average density trends, 1967–2007, derived from orbits of 5000 near-Earth objects, *Geophys. Res. Lett.*, *35*, L05101, doi:10.1029/2007GL032809.

Fritts, D. C. (1984), Gravity wave saturation in the middle atmosphere: A review of theory and observations, *Rev. Geophys. Space Phys.*, *22*(3), 275–308.

Fukao, S., M. D. Yamanaka, N. Ao, W. K. Hocking, T. Sato, M. Yamamoto, T. Nakamura, T. Tsuda, and S. Kato (1994), Seasonal variability of ver-

tical eddy diffusivity in the middle atmosphere: 1. Three-year observations by the middle and upper atmosphere radar, *J. Geophys. Res.*, *99*, 18,973–18,987.

Fuller-Rowell, T. J. (1998), The "thermospheric spoon": A mechanism for the semiannual density variation, *J. Geophys. Res.*, *103*, 3951–3956.

Garcia, R. R., and S. Solomon (1985), The effect of breaking gravity waves on the dynamics and chemical composition of the mesosphere and lower thermosphere, *J. Geophys. Res.*, *90*, 3850–3868.

Hagan, M. E., and J. M. Forbes (2002), Migrating and nonmigrating diurnal tides in the middle and upper atmosphere excited by tropospheric latent heat release, *J. Geophys. Res.*, *107*(D24), 4754, doi:10.1029/2001JD001236.

Hagan, M. E., and J. M. Forbes (2003), Migrating and nonmigrating semidiurnal tides in the upper atmosphere excited by tropospheric latent heat release, *J. Geophys. Res.*, *108*(A2), 1062, doi:10.1029/2002JA009466.

Hedin, A. E. (1983), A revised thermospheric model based on mass spectrometer and incoherent scatter data: MSIS-83, *J. Geophys. Res.*, *88*, 10,170–10,188.

Hedin, A. E. (1987), MSIS-86 thermosphere model, *J. Geophys. Res.*, *92*, 4649–4662.

Hedin, A. E. (1991), Extension of the MSIS thermosphere model into the middle and lower atmosphere, *J. Geophys. Res.*, *96*, 1159–1172.

Hedin, A. E., and D. Alcaydé (1974), Comparison of atomic oxygen measurements by incoherent scatter and satellite-borne mass spectrometer techniques, *J. Geophys. Res.*, *79*, 1579–1581.

Hedin, A. E., et al. (1977a), A global thermospheric model based on mass spectrometer and incoherent scatter data, MSIS 1, N_2 density and temperature, *J. Geophys. Res.*, *82*, 2139–2147.

Hedin, A. E., C. A. Reber, G. P. Newton, N. W. Spenser, H. C. Brinton, H. G. Mayr, and W. E. Potter (1977b), A global thermospheric model based on mass spectrometer and incoherent scatter data, MSIS 2, composition, *J. Geophys. Res.*, *82*, 2148–2156.

Heelis, R. A., J. K. Lowell, and R. W. Spiro (1982), A model of the high-latitude ionospheric convection pattern, *J. Geophys. Res.*, *87*, 6339–6345.

Hines, C. O. (1970), Eddy diffusion coefficients due to instabilities in internal gravity waves, *J. Geophys. Res.*, *75*, 3937–3939.

Hirota, I. (1980), Observational evidence of the semiannual oscillation in the tropical middle-atmosphere—A review, *Pure Appl. Geophys.*, *118*, 217–238.

Hitchman, M. H., and C. B. Leovy (1986), Evolution of the zonal mean state in the equatorial middle atmosphere during October 1978–May 1979, *J. Atmos. Sci.*, *43*, 3159–3176.

Hodges, R. R. (1969), Eddy diffusion coefficients due to instabilities in internal gravity waves, *J. Geophys. Res.*, *74*, 4087–4090.

Huang, F. T., H. G. Mayr, C. A. Reber, J. M. Russell, M. Mlynczak, and J. G. Menel (2006), Stratospheric and mesospheric temperature variations for the quasi-biennial and semiannual (QBO and SAO) oscillations based on measurements from SABER (TIMED) and MLS (UARS), *Ann. Geophys.*, *24*(8), 2131–2149.

Immel, T. J., E. Sagawa, S. L. England, S. B. Henderson, M. E. Hagan, S. B. Mende, H. U. Frey, C. M. Swenson, and L. J. Paxton (2006), Control of equatorial ionospheric morphology by atmospheric tides, *Geophys. Res. Lett.*, *33*, L15108, doi:10.1029/2006GL026161.

Jacchia, L. G. (1965), Static diffusion models of the upper atmosphere with empirical temperature profiles, *Smithson. Contrib. Astrophys.*, *8*, 215–257.

Jacchia, L. G. (1971), Semiannual variation in the heterosphere: A re-appraisal, *J. Geophys. Res.*, *76*, 4602–4607.

Jacchia, L. G. (1974), Variations in thermospheric composition: A model based on mass spectrometer and satellite drag data, *J. Geophys. Res.*, *79*, 1923–1927.

Jacchia, L. G. (1977), Thermospheric temperature, density, and composition: New models, *Smithson. Astrophys. Obs. Spec. Rep. 375*, 1–106.

Jacchia, L. G., J. W. Slowey, and U. von Zahn (1976), Latitudinal changes of composition in the disturbed thermosphere from Esro 4 measurements, *J. Geophys. Res.*, *81*, 36–42.

Johnson, F. S., and B. Gottlieb (1970), Eddy mixing and circulation at ionospheric levels, *Planet. Space Sci.*, *18*, 1707–1718.

Keating, G. M., R. H. Tolson, and M. S. Bradford (2000), Evidence of long-term global decline in the Earth's thermospheric densities apparently related to anthropogenic effects, *Geophys. Res. Lett.*, *27*, 1523–1526.

Khattatov, B. V., M. A. Geller, and V. A. Yubin (1997), Diurnal migrating tides as seen by the high-resolution Doppler imager/UARS: 2. Monthly mean global zonal and vertical velocities, pressure, temperature, and inferred dissipation, *J. Geophys. Res.*, *102*, 4423–4435.

Kirchhoff, V. W. J. H., and B. R. Clemesha (1983), Eddy diffusion coefficients in the lower thermosphere, *J. Geophys. Res.*, *88*, 5765–5768.

Lindzen, R. S. (1967), Thermally driven diurnal tide in the atmosphere, *Q. J. R. Meterol. Soc.*, *93*, 18–42.

Lindzen, R. S. (1971), Tides and gravity waves in the upper atmosphere, in *Mesoapheric Models and Related Experiments*, edited by G. Fiocco, 198 pp., Springer, New York.

Lindzen, R. S. (1981), Turbulence and stress owing to gravity wave and tidal breakdown, *J. Geophys. Res.*, *86*, 9707–9714.

Lübken, F. J. (1997), Seasonal variation of turbulent energy dissipation rates at high latitudes as determined by in situ measurements of neutral density fluctuations, *J. Geophys. Res.*, *102*, 13,441–13,456.

Marcos, F. A., J. O. Wise, M. J. Kendra, N. J. Grossbard, and B. R. Bowman (2005), Detection of a long-term decrease in thermospheric neutral density, *Geophys. Res. Lett.*, *32*, L04103, doi:10.1029/2004GL021269.

Marsh, D. R., R. R. Garcia, D. E. Kinnison, B. A. Boville, F. Sassi, S. C. Solomon, and K. Matthes (2007), Modeling the whole atmosphere response to solar cycle changes in radiative and geomagnetic forcing, *J. Geophys. Res.*, *112*, D23306, doi:10.1029/2006JD008306.

Mayr, H. G., and H. Volland (1971), Semiannual variation in the neutral composition, *Ann. Geophys.*, *27*, 513–522.

Mayr, H. G., and H. Volland (1972), Theoretical model for the latitude dependence of the thermospheric annual and semiannual variations, *J. Geophys. Res.*, *77*, 6774–6790.

Mayr, H. G., I. Harris, and N. W. Spenser (1978), Some properties of upper atmospheric dynamics, *Rev. Geophys. Space Phys.*, *16*, 539–565.

Mendillo, M., H. Rishbeth, R. G. Roble, and J. Wroten (2002), Modelling F2-layer seasonal trends and day-to-day variability driven by coupling with the lower atmosphere, *J. Atmos. Sol. Terr. Phys.*, *64*, 1911–1931.

Mendillo, M., C.-L. Huang, X.-Q. Pi, H. Rishbeth, and R. R. Meier (2005), The global asymmetry in ionospheric total content (2005), *J. Atmos. Sol. Terr. Phys.*, *67*, 1377–1387.

Paetzold, H. K., and H. Zschörner (1961), An annual and a semiannual variation of the upper air density, *Pure Appl. Geophys.*, *48*, 85–92.

Picone, J. M., A. E. Hedin, D. P. Drob, and A. C. Aikin (2002), NRLMSISE-00 empirical model of the atmosphere: Statistical comparisons and scientific issues, *J. Geophys. Res.*, *107*(A12), 1468, doi:10.1029/2002JA009430.

Potter, W. E., D. C. Kayser, H. C. Brinton, L. H. Brace, and M. Oppenheimer (1977), Comparison of measured and calculated thermospheric molecular oxygen densities, *J. Geophys. Res.*, *82*, 5243–5248.

Prölss, G. W., and U. von Zahn (1977), On the global morphology of negative ionospheric storms, *Space Res.*, *17*, 433–438.

Qian, L., R. G. Roble, S. C. Solomon, and T. J. Kane (2006), Calculated and observed climate change in the thermosphere, and a prediction for solar cycle 24, *Geophys. Res. Lett.*, *33*, L23705, doi:10.1029/2006GL027185.

Rao, D. N., M. V. Ratnam, T. N. Rao, and S. V. B. Rao (2001), Seasonal variation of vertical eddy diffusivity in the troposphere, lower stratosphere and mesosphere over a tropical station, *Ann. Geophys.*, *19*, 975–984.

Remsberg, E. E., P. P. Bhatt, and L. E. Deaver (2002), Seasonal and longer-term variations in middle atmosphere temperature from HALOE on UARS, *J. Geophys. Res.*, *107*(D19), 4411, doi:10.1029/2001JD001366.

Richards, P. G., J. A. Fennelly, and D. G. Torr (1994), EUVAC: A solar EUV flux model for aeronomic calculations, *J. Geophys. Res.*, *99*, 8981–8992.

Richmond, A. D. (1995), Ionospheric electrodynamics using magnetic apex coordinates, *J. Geomagn. Geoelectr.*, *47*, 191–212.

Richmond, A. D., E. C. Ridley, and R. G. Roble (1992), A thermosphere/ionosphere general circulation model with coupled electrodynamics, *Geophys. Res. Lett.*, *19*, 601–604.

Rishbeth, H., and I. C. F. Müller-Wodarg (1999), Vertical circulation and thermospheric composition: A modelling study, *Ann. Geophys.*, *17*, 794–805.

Rishbeth, H., and I. C. F. Müller-Wodarg (2006), Why is there more ionosphere in January than in July? The annual asymmetry in the F2-layer, *Ann. Geophys.*, *24*, 3293–3311.

Rishbeth, H., I. C. F. Müller-Wodarg, L. Zou, T. J. Fuller-Rowell, G. H. Millward, R. J. Moffett, D. W. Idenden, and A. D. Aylward (2000a), Annual and semiannual variations in the ionospheric F2-layer. II: Physical discussion, *Ann. Geophys.*, *18*, 945–956.

Rishbeth, H., K. J. F. Sedgemore-Schulthess, and T. Ulich (2000b), Semiannual and annual variations in the height of the ionospheric F2-peak, *Ann. Geophys.*, *18*, 285–299.

Roble, R. G. (1995), Energetics of the mesosphere and thermosphere, in *The Upper Mesosphere and Lower Thermosphere: A Review of Experiment and Theory*, Geophys. Monogr. Ser., vol. 87, edited by R. M. Johnson and T. L. Killeen, pp. 1–21, AGU, Washington, D. C.

Roble, R. G., and R. E. Dickinson (1989), How will changes in carbon dioxide and methane modify the mean structure of the mesosphere and thermosphere?, *Geophys. Res. Lett.*, *16*, 1441–1444.

Roble, R. G., and E. C. Ridley (1987), An auroral model for the NCAR thermosphere general circulation model (TGCM), *Ann. Geophys.*, *5A*(6), 369–382.

Roble, R. G., and E. C. Ridley (1994), Thermosphere-ionosphere-mesosphere-electrodynamics general circulation model (TIME-GCM): Equinox solar minimum simulations (30–500 km), *Geophys. Res. Lett.*, *21*, 417–420.

Roble, R. G., E. C. Ridley, and R. E. Dickinson (1982), Global circulation and temperature structure of the thermosphere with high latitude convection, *J. Geophys. Res.*, *87*, 1599c.

Roble, R. G., E. C. Ridley, and R. E. Dickinson (1987), On the global mean structure of the thermosphere, *J. Geophys. Res.*, *92*, 8745–8758.

Roble, R. G., E. C. Ridley, A. D. Richmond, and R. E. Dickinson (1988), A coupled thermosphere/ionosphere general circulation model, *Geophys. Res. Lett.*, *15*, 1325–1328.

Sasi, M. N., and L. Vijayan (2001), Turbulence characteristics in the tropical mesosphere as obtained by MST radar at Gadanki (13.5°N, 79.2°E), *Ann. Geophys.*, *19*, 1019–1025.

Shimazaki, T. (1971), Effective eddy diffusion coefficient and atmospheric composition in the lower thermosphere, *J. Atmos. Terr. Phys.*, *33*, 1383–1401.

Schuchardt, K. G. H., and P. W. Blum (1977), Correlation between the homopause height and density variations in the upper atmospheres, *Space Res.*, *13*, 335–340.

Solomon, S. C., and L. Qian (2005), Solar extreme-ultraviolet irradiance for general circulation models, *J. Geophys. Res.*, *110*, A10306, doi:10.1029/2005JA011160.

Strickland, D. J., R. R. Meier, R. L. Walterscheid, A. B. Christensen, L. J. Paxton, D. Morrison, J. D. Craven, and G. Crowley (2004), Quiet-time seasonal behavior of the thermosphere seen in the far ultraviolet dayglow, *J. Geophys. Res.*, *109*, A01302, doi:10.1029/2003JA010220.

Taeusch, D. R., G. R. Carignan, and C. A. Reber (1971), Neutral composition variation above 400 km during a magnetic storm, *J. Geophys. Res.*, *76*, 8318–8325.

Walterscheid, R. L. (1982), The semiannual oscillation in the thermosphere as a conduction mode, *J. Geophys. Res.*, *87*, 10,527–10,535.

Woods, T. N., F. G. Eparvier, S. M. Bailey, P. C. Chamberlin, J. Lean, G. J. Rottman, S. C. Solomon, W. K. Tobiska, and D. L. Woodraska (2005), Solar EUV Experiment (SEE): Mission overview and first results, *J. Geophys. Res.*, *110*, A01312, doi:10.1029/2004JA010765.

Wu, Q., D. A. Ortland, T. L. Killeen, R. G. Roble, M. E. Hagan, H.-L. Liu, S. C. Solomon, J. Xu, W. R. Skinner, and R. J. Niciejewski (2008), Global distribution and interannual variations of mesospheric and lower thermospheric neutral wind diurnal tide: 1. Migrating tide, *J. Geophys. Res.*, *113*, A05308, doi:10.1029/2007JA012542.

Zhang, Y., and L. J. Paxton (2008), An empirical Kp-dependent global auroral model based on TIMED/GUVI FUV data, *J. Atmos. Sol. Terr. Phys.*, *70*, 1231, doi:10.1016/j.jastp.2008.03.008.

Zhang, Y., L. J. Paxton, D. Morrison, B. Wolven, H. Kil, C.-I. Meng, S. B. Mende, and T. J. Immel (2004), O/N_2 changes during 1–4 October 2002 storms: IMAGE SI-13 and TIMED/GUVI observations, *J. Geophys. Res.*, *109*, A10308, doi:10.1029/2004JA010441.

───────────────

T. J. Kane, Department of Electrical Engineering, Pennsylvania State University, University Park, PA 16802, USA.

L. Qian and S. C. Solomon, High Altitude Observatory, National Center for Atmospheric Research, 3080 Center Green Drive, Boulder, CO 80301, USA. (lqian@ucar.edu)